Dalton Transactions

ROYAL SOCIETY OF CHEMISTRY

PERSPECTIVE

View Article Online
View Journal

Cite this: DOI: 10.1039/d5dt01501d

Dynamic functions of bis- and tris(saloph) cobalt(III) structures based on axial coordination

Shigehisa Akine [a,b]

This review article focuses on the functionalization and dynamic functional switching of low-spin d^6 cobalt(III) complexes derived from various oligo(saloph) structures, such as bis(saloph) macrocycles and tris(saloph) cage complexes (H_2saloph = *N*,*N*′-disalicylidene-*o*-phenylenediamine). The bis(saloph) dicobalt(III) complexes with methylene- or phenylene-bridged ligands exhibit reversible redox-driven structural switching, in which the axial functional ligands dissociate and reassociate in response to the Co^{III}/Co^{II} interconversion. The ether-bridged macrocyclic bis(saloph) cobalt(III) complexes show excellent cation binding affinity at the central O_6 binding site, which is significantly influenced by the nature of the axial ligands at the cobalt centers. In particular, an anion-capped structure leads to the formation of a unique metastable host–guest complex, enabling stimuli-responsive behavior upon external triggering. Post-metalation ligand exchange with anionic ligands and bridging diamine ligands provides a versatile strategy for structural and functional tuning of these macrocyclic hosts. In some complexes, the ligand exchange reactivity and the guest binding affinity enhance each other. A helical tris(saloph) cobalt(III) cryptand exhibits dynamic *P*/*M* chirality interconversion *via* the axial ligand exchange involving achiral or chiral amines, allowing precise control over the chirality inversion rates and enabling a unique transient chirality inversion during racemization. Furthermore, closed-cage metallocryptands bearing bridging diamine ligands effectively suppress the guest uptake/release kinetics. Thus, the introduction, removal, and exchange of axial ligands (X) in the $[Co(saloph)X_2]^+$-type units have been successfully employed for the functionalization and dynamic switching of metallohosts and metallo-supramolecular structures.

Received 25th June 2025,
Accepted 21st August 2025

DOI: 10.1039/d5dt01501d

rsc.li/dalton

1. Introduction

The salen ligand†[1] and its phenylene analog, the saloph ligand,‡[1] are versatile tetradentate chelate ligands that provide a planar N_2O_2 coordination environment (Fig. 1a). Some of the resulting transition metal complexes have been used as catalysts,[2] liquid crystals,[3] and sensors,[4] and are known to exhibit unique magnetic[5] and optical properties,[6] as well as biological activities.[7] In addition to simple monomeric structures, many oligomeric compounds containing multiple salen units have been developed,[8,9] and their material applications[10] and catalytic functions[11] have been studied. These include macrocyclic oligomers,[8,9] as well as acyclic oligomers[12] and molecular cages.[13] In particular, cyclic oligomers and cage structures are advantageous because they can be obtained in relatively high yields, thanks to the dynamic nature of the imine C=N double bonds.[14] Some of these compounds exhibit unique host–guest binding affinities toward molecular and ionic guest species,[9] taking advantage of the rigid and shape-persistent nature of the salen/saloph complex structures, which arises from their well-defined chelate coordination motifs.

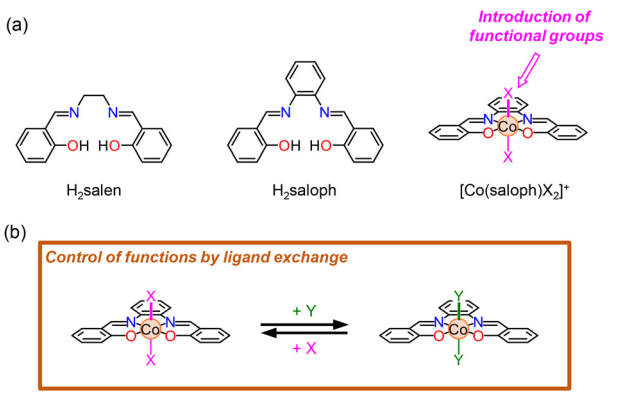

Fig. 1 (a) Chemical structures of H_2salen, H_2saloph, and $[Co(saloph)X_2]^+$. Functional groups can be introduced as axial ligands *X*. (b) *X*/*Y* axial ligand exchange in $[Co(saloph)X_2]^+$ structures, allowing for tunable properties at the axial positions.

[a]*Nano Life Science Institute (WPI-NanoLSI), Kanazawa University, Kakuma-machi, Kanazawa 920-1192, Japan. E-mail: akine@se.kanazawa-u.ac.jp*
[b]*Graduate School of Natural Science and Technology, Kanazawa University, Kakuma-machi, Kanazawa 920-1192, Japan*

† H_2salen = *N*,*N*′-disalicylideneethylenediamine.
‡ H_2saloph = *N*,*N*′-disalicylidene-*o*-phenylenediamine.

Among the metals that can be incorporated into these oligo(salen)/-(saloph) structures for metallohosts and metallosupramolecular systems, those with a d^8 electron configuration, such as nickel(II)[15] and palladium(II),[16] are particularly advantageous. Their square-planar geometry aligns well with the planar N_2O_2 coordination environment provided by the salen/saloph ligands. Metalation of these ligands yields rigid square planar complexes through the simultaneous formation of four coordination bonds, which facilitates the predictable and selective formation of shape-persistent structures. In addition, the resulting d^8 square-planar complexes are diamagnetic. The use of diamagnetic metals is, in fact, essential for the investigation of metal-containing supramolecular and host–guest structures, as it allows for NMR measurements for structural elucidation and detailed analysis of host–guest binding.

In contrast to the square-planar metal ions, pentacoordinate metal centers situated in the salen/saloph coordination pocket can accommodate an additional monodentate ligand. For example, parent salen/saloph ligands are known to form mononuclear pentacoordinate complexes formulated as [Zn(salen)X]/[Zn(saloph)X] (X = H_2O, py, *etc.*)[17] or dimeric complexes $[Zn_2(salen)_2]$/$[Zn_2(saloph)_2]$ in which one of the phenoxo oxygen atoms occupies the apical position of the counterpart Zn^{2+}.[18] This fifth coordination has been utilized for the construction, structural conversion, and functionalization of various types of multi-metal self-assembled structures.[19–21]

Analogously, hexacoordinate complexes, [M(salen)X_2]/[M(saloph)X_2], can be obtained by introducing two additional monodentate ligands (X) to the metal centers in the salen/saloph coordination site. In fact, the salen/saloph ligands can accommodate various metal ions with an octahedral geometry, which is the most common and ubiquitous coordination structure adopted by a wide range of transition metal ions. In most cases, the N_2O_2 donor set of the salen/saloph ligands occupies four equatorial positions around the octahedral metal ion. Accordingly, the two X ligands in the [M(salen)X_2]/[M(saloph)X_2] complexes occupy *trans* positions to each other, located at the axial positions relative to the MN_2O_2 plane in the [M(salen)]/[M(saloph)] structures (Fig. 1a).[22]

In particular, among various salen/saloph complexes containing an octahedral metal ion, the cobalt(III) complexes, [Co(salen)X_2]$^+$/[Co(saloph)X_2]$^+$,[23,24] offer significant advantages. Owing to the large ligand field splitting originating from the low-spin d^6 electron configuration, diamagnetic complexes are usually obtained exclusively and predictably, which facilitates investigation based on NMR spectroscopy. In addition, these low-spin cobalt(III) complexes are generally inert and stable, which allows various types of site-selective functionalizations at the axial positions without loss of the central cobalt(III) ion from the salen/saloph structures. Ligand exchange occurs slowly and only at the two axial X positions in the [Co(salen)X_2]$^+$/[Co(saloph)X_2]$^+$ structures, on a timescale of minutes to hours,[25] owing to their inert nature (Fig. 1b). This reactivity is useful for the slow, time-dependent control of functions in the multi-metal structures.[26] Although kinetic inertness often hampers the integration of dynamic functions into metal complexes, [Co(salen)]/[Co(saloph)] structures offer a distinct advantage: their axial positions remain sufficiently reactive while the equatorial CoN_2O_2 core maintains structural integrity. This spatially controlled reactivity enables the rational design of dynamic, switchable systems based on inert cobalt(III) centers.

Cobalt(III) complexes are particularly suited for functionally relevant structural transformations *via* selective axial ligand exchange, even though other transition metal complexes such as Pd, Pt, and Fe also exhibit kinetic inertness. Furthermore, the redox activity of cobalt(III), especially the Co^{III}/Co^{II} couple, offers additional opportunities for external control and switching of functions,[27] which is less accessible in Pd, Pt, Zn, or Fe systems. Indeed, a wide range of cobalt(III)-based redox-responsive functional molecules and supramolecular architectures have been developed, demonstrating the broad versatility and growing importance of switchable metal-containing structures.[28]

This review article focuses on the functionalization and dynamic switching of the low-spin d^6 cobalt(III) complexes derived from various kinds of oligo(saloph) structures, such as bis(saloph) ligands (H_4L^1, H_4L^2, H_4L^3, H_4L^4) and the tris(saloph) cage (H_6L^5) (Fig. 2). In particular, introduction, removal, and exchange of the axial ligands X in the [Co(salen)X_2]$^+$/[Co(saloph)X_2]$^+$ structures[26] have been efficiently employed for functionalization and the dynamic functional switching of metallohosts and metallo-supramolecular structures incorporating cobalt(III) centers.

Shigehisa Akine

Shigehisa Akine received his Ph. D. in 2000 from the University of Tokyo under the supervision of Prof. Takayuki Kawashima, then worked as a research associate with Prof. Tatsuya Nabeshima at the University of Tsukuba. He became assistant professor in 2004 and associate professor in 2008. In 2013, he joined Kanazawa University as a full professor and in 2017 became a principal investigator at the Nano Life Science Institute (WPI-NanoLSI). His research focuses on kinetic control of structural conversions in responsive molecules, especially in host–guest, supramolecular, coordination, and organic chemistry.

2. Functions of bis(saloph) cobalt(III) complexes based on axial coordination

2.1. Methylene-bridged macrocyclic bis(saloph) dicobalt(III) complexes for redox-driven structural switching

A bis(saloph) macrocyclic ligand, H_4L^1 (Fig. 2),[29] in which two H_2saloph motifs are connected by two methylene linkers to

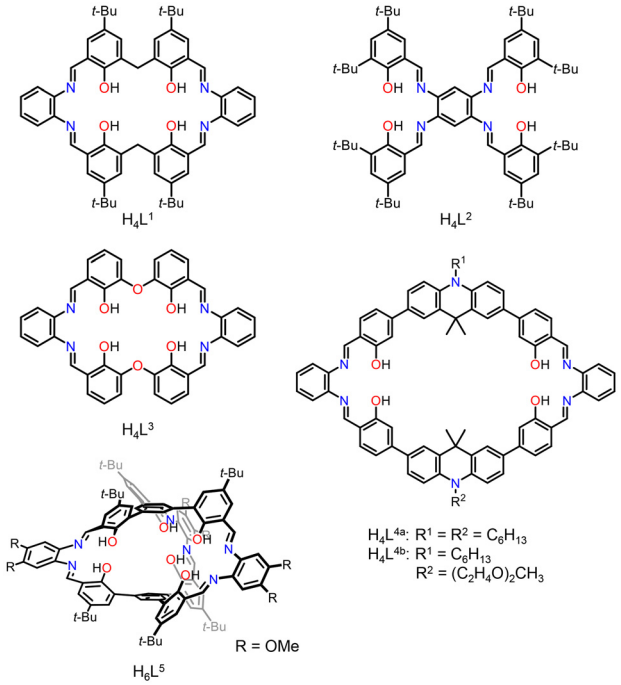

Fig. 2 Chemical structures of bis(saloph) compounds, H_4L^1, H_4L^2, H_4L^3, H_4L^4, and tris(saloph) cage H_6L^5.

form a macrocyclic framework, was synthesized. A series of doubly bridged dicobalt(III) complexes, L^1Co_2(**DA*n***)$_2$, was prepared by reacting H_4L^1 with cobalt(II) acetate in the presence of various diamine ligands (**DA*n*** = **DA1–DA6**) under aerobic conditions (Fig. 3a).[30] These complexes were characterized by spectroscopic methods and X-ray crystallography, revealing dinuclear structures featuring two diamagnetic cobalt(III) ions bridged by diamine ligands, such as alkanediamines **DA1–DA4** with varying methylene chain lengths (Fig. 3a). The use of oligo(ether) diamines, **DA5** and **DA6**, introduced potential cation binding sites into the dicobalt(III) macrocycle, analogous to crown ethers.

While the cobalt(III) ions in the L^1Co_2(**DA*n***)$_2$ complex prefer a hexacoordinate octahedral geometry (Fig. 3a), reduction to

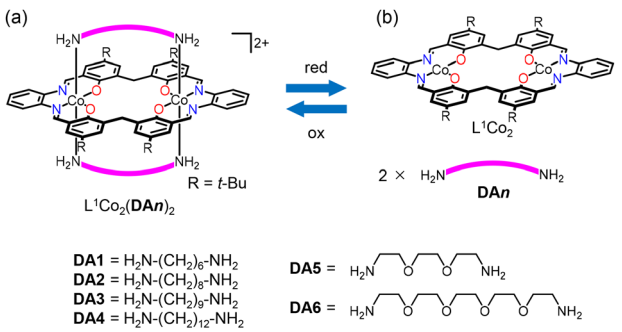

Fig. 3 Redox switching of dinuclear complexes L^1Co_2(**DA*n***)$_2$. (a) The oxidized state with octahedral cobalt(III) ions. (b) The reduced state with tetracoordinate cobalt(II) ions.

cobalt(II) leads to a less coordinated geometry (Fig. 3b). This Co^{III}/Co^{II} redox transformation can be exploited to switch between the bound and unbound states of the axial ligands at the cobalt centers. Electrochemical measurements exhibited redox waves with large peak separations, suggesting that the redox processes are accompanied by significant changes in coordination geometry.[30] Specifically, the $Co^{III} \rightarrow Co^{II}$ reduction occurs in the hexacoordinate state with bridging diamine ligands, whereas the $Co^{II} \rightarrow Co^{III}$ oxidation occurs in a tetracoordinate state lacking the diamine ligands (Fig. 3b). The reversible structural transformation between these two states was further confirmed by electrolytic absorption spectroscopy as well as mass spectrometry.

Thus, the doubly bridged structure can be constructed and destructed by association/dissociation of the axially coordinating diamine ligands **DA*n*** in response to redox changes. This would significantly change the host–guest binding behavior in the polyether-based cavities of L^1Co_2(**DA5**)$_2$ and L^1Co_2(**DA6**)$_2$. However, these dinuclear cobalt(III) complexes did not exhibit any binding affinity for alkali metal ions such as Li^+, Na^+, or K^+.[29] This may be attributed to the positive charge of the dicationic L^1Co_2 core, which experiences strong electrostatic repulsion with cationic guests.

2.2. Phenylene-bridged bis(saloph) dicobalt(III) complexes for redox-driven structural switching

The acyclic bis(saloph) ligand, H_4L^2 (Fig. 2), in which two H_2saloph units share a single phenylenediamine subunit, is known to form a series of dinuclear complexes where the two metal centers are electronically coupled.[20,24,31] This H_4L^2 ligand was used to prepare the dinuclear cobalt(III) complex L^2Co_2(**B1**)$_4$, which features four crown ether subunits at the axial positions of the cobalt(III) centers (Fig. 4).[32] The complex was synthesized by the reaction of H_4L^2 with cobalt(II) acetate in the presence of 4-aminomethylbenzo-15-crown-5 (**B1**) under aerobic conditions.

Since each face of the L^2Co_2(**B1**)$_4$ complex functions as a bis(15-crown-5) host capable of binding a cationic guest in a sandwich fashion, the complex was expected to bind two K^+ ions on both faces to form a 1 : 2 (host/guest) complex. However, spectroscopic measurements revealed that this L^2Co_2(**B1**)$_4$ complex exhibits K^+ binding with 1 : 1 stoichiometry, as confirmed by Job plot analysis and mass spectrometry. This binding behavior can be rationalized by the molecular deformation caused by the first guest binding in a $[(15\text{-crown-5})_2K]^+$ sandwich fashion, which may increase the distance between the two crown ether moieties on the opposite face, thereby suppressing the second K^+ binding. This L^2Co_2(**B1**)$_4$ complex also undergoes a reversible Co^{III}/Co^{II} redox interconversion, accompanied by the association/dissociation of the axially coordinating crown ether subunits **B1** (Fig. 4).[32]

The Co^{III}/Co^{II} redox interconversion of the same dinuclear L^2Co_2 motif was also exploited for the reversible association/dissociation of dendrimer subunits **G3**. The dinuclear complex L^2Co_2(**G3**)$_4$, which contains four dendrimer subunits **G3** (Fig. 5),[33] was expected to undergo Co^{III}/Co^{II} redox switching

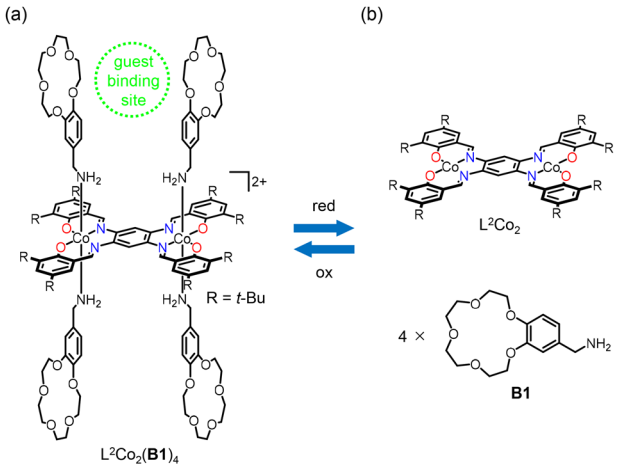

Fig. 4 Redox-driven structural conversion of crown-ether-functionalized complex L^2Co_2(**B1**)$_4$. (a) Oxidized state and (b) reduced state. Only the oxidized form L^2Co_2(**B1**)$_4$ can bind a K^+ ion in a sandwich fashion, enabling redox-switchable guest binding.

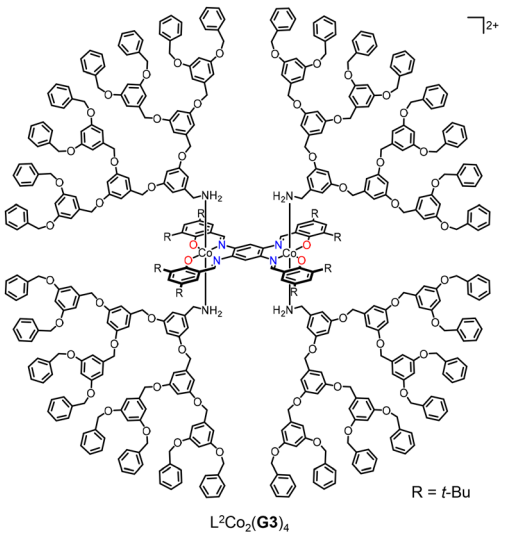

Fig. 5 Chemical structure of the dendrimer-functionalized dinuclear complex L^2Co_2(**G3**)$_4$.

accompanied by the reversible binding of the dendrimer subunits **G3**. However, under electrochemical conditions, L^2Co_2(**G3**)$_4$ did not exhibit efficient redox switching, likely due to the steric bulkiness of the dendrimer subunits **G3**. Instead, photo-driven redox reactions proved effective: upon photoirradiation ($\lambda \geq 420$ nm) in a degassed DMF solution containing triethanolamine as a sacrificial electron donor, the complex was reduced to a tetracoordinate dicobalt(II) species. This reduced form can be re-oxidized by air exposure to regenerate the initial hexacoordinate dicobalt(III) complex. Thus, despite the steric hindrance from the bulky dendrimer subunits, reversible association/dissociation of the dendrimer subunits in L^2Co_2(**G3**)$_4$ was successfully achieved *via* photo-driven redox switching.

2.3. Ether-bridged bis(saloph) dicobalt(III) macrocycles for controlled guest binding

An ether-bridged bis(saloph) macrocycle, H_4L^3 (Fig. 2), which is an oxygen analogue of the methylene-bridged bis(saloph) macrocycle H_4L^1, was synthesized.[34] Owing to the ether linkages, the metalated form, L^3M_2, features an 18-crown-6-like central binding cavity surrounded by six oxygen donor atoms, which exhibit excellent binding affinity for cationic guest species. For example, the nickel(II) metallohost L^3Ni_2 (Fig. 6a) strongly binds to Na^+ to form a 1 : 1 host–guest complex and interacts with larger alkali metal ions (K^+, Rb^+, Cs^+) to afford unique stacked structures.[34–38] This higher binding affinity arises from the combination of negatively polarized phenoxo oxygen atoms and the well pre-organized structure of the metallohosts. This section focuses on the guest binding behavior of the hexacoordinate cobalt(III) analogues $L^3Co_2A_4$ (Fig. 6b), which have four primary amine ligands **A** at the axial positions of the cobalt(III) centers.

Since the dinuclear cobalt(III) metallohosts $L^3Co_2A_4$ are dicationic, they were expected to show a poor cation binding affinity due to electrostatic repulsion, especially in comparison to the non-charged nickel(II) analogue L^3Ni_2. Contrary to expectations, however, the cobalt(III) metallohost $L^3Co_2(MeNH_2)_4$, bearing four methylamine ligands, showed excellent binding affinity toward various cationic guests, such as a monovalent cation, Na^+ ($K_a = 8.5 \times 10^6$ M^{-1}), and even a multivalent cation, La^{3+} ($K_a = 2.4 \times 10^6$ M^{-1}).[39] In the crystal structure of the Na^+ inclusion complex, $L^3Co_2(MeNH_2)_4Na$, the Na^+ ion is located precisely at the center of the O_6 binding site (Fig. 7a). The triflate counter anions not only directly coordinate to the Na^+ ion but also form hydrogen bonds with the methylamine NH_2 groups on both faces of the macrocycle, resulting in a unique anion-capped structure (Fig. 7b).[39] These noncovalent interactions appear to contribute not only to the strong cation binding, but also to blocking guest entry/exit, acting like a cap or lid on a container.

In fact, the guest uptake/release rates of the metallohost $L^3Co_2(MeNH_2)_4$ were found to be slow on the ^1H NMR time scale for cationic guests such as Na^+, K^+, and Ca^{2+}. Notably, the uptake of the La^{3+} ion was particularly slow ($k_{in} \approx 10^{-2}$ M^{-1} s^{-1}), requiring nearly 100 h to reach completion. This remarkably slow uptake was attributed to the anion-capped structure,

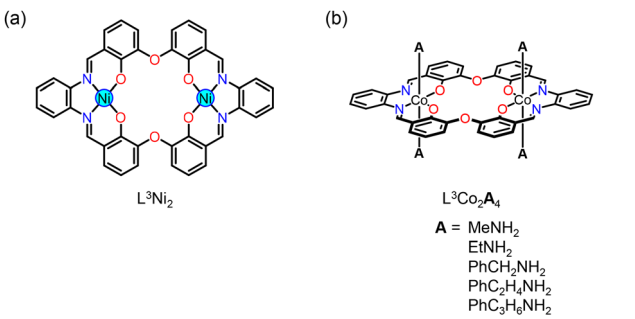

Fig. 6 Chemical structures of (a) L^3Ni_2 and (b) $L^3Co_2A_4$.

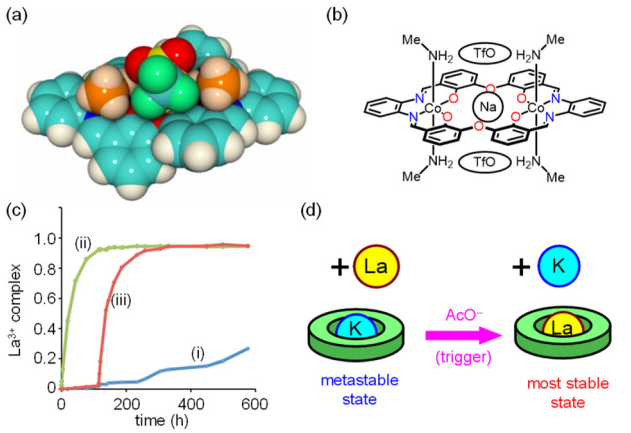

Fig. 7 (a) X-ray crystal structure of $L^3Co_2(MeNH_2)_4Na$. The two TfO^- counter anions are also shown. (b) Schematic drawing of the anion-capped structure of the host–guest complex, $L^3Co_2(MeNH_2)_4Na$. (c) Plots of mole fractions of the La^{3+} complex *versus* time after the addition of K^+ in CD_3OD: (i) in the absence of AcO^-; (ii) in the presence of AcO^-; (iii) guest exchange was initiated when AcO^- was added as a trigger after 120 h. (d) Conversion of the metastable state [K^+ complex + unbound La^{3+}] into the thermodynamically most stable state [La^{3+} complex + unbound K^+] triggered by AcO^-. Adapted in part with permission from ref. 39.

as the uptake rate was found to depend significantly on the nature of counter anions.

This anion-capped structure also contributed to the deceleration of guest exchange in the metallohost $L^3Co_2(MeNH_2)_4$. A compelling demonstration is the formation of a metastable host–guest complex, that is, a kinetically trapped state in which a weaker guest is preferentially bound within the host cavity, leaving a stronger guest unbound. From a thermodynamic viewpoint, the metallohost showed a lower affinity for K^+ (K_a = 1.1 × 10^6 M^{-1}) than for La^{3+} (K_a = 2.4 × 10^6 M^{-1}). However, when K^+ and La^{3+} were simultaneously added, K^+ was selectively taken up for kinetic reasons. Guest exchange to the thermodynamically favored La^{3+} complex was not observed even after 2 weeks (Fig. 7c(i)), indicating that the guest exchange was almost completely kinetically suppressed. Typically, guest binding in simple crown ethers is fast enough that the thermodynamically most stable complex is always selectively formed. In this context, the cobalt(III) metallohost $L^3Co_2(MeNH_2)_4$ gives the first metastable host–guest complex derived from a simple macrocyclic host (Fig. 7d).[39,40]

Such a metastable state retains the potential to transition to the thermodynamically most stable structure at any time when triggered. In the aforementioned case, the mixture of the K^+ complex with unbound La^{3+} remained in a kinetically trapped metastable state, where the conversion to the thermodynamically most stable state was suppressed, but this conversion was accelerated by the addition of acetate ion as a trigger (Fig. 7c(ii), (iii) and d). This represents a new type of on-demand, stimuli-responsive function that exploits the long-lived yet transformable nature of a metastable host–guest complex.

Thus, the guest uptake/release rates of the metallohost $L^3Co_2(MeNH_2)_4$ were found to be significantly decelerated by its anion-capped structure. These rates were also expected to be influenced by the structure of the amine ligands **A** coordinating to the cobalt(III) ions. In order to clarify this effect, a series of dinuclear metallohosts $L^3Co_2\mathbf{A}_4$, each bearing four primary monoamine ligands (**A** = $EtNH_2$, $PhCH_2NH_2$, $PhC_2H_4NH_2$, $PhC_3H_6NH_2$) with or without a phenyl group remote from the O_6 binding cavity, were synthesized (Fig. 6b). All these metallohosts exhibited a consistent selectivity trend among alkali metal ions: $Na^+ > K^+ > Rb^+ > Cs^+$. This trend was primarily attributed to differences of up to ~500 000-fold in the release rate constants k_{out}, following the order of $Na^+ < K^+ < Rb^+ < Cs^+$.[41]

The structural variation in the amine ligands **A** also affected the binding behavior in both thermodynamic and kinetic aspects (Table 1). For example, the binding constants of $L^3Co_2\mathbf{A}_4$ (**A** = $EtNH_2$, $PhCH_2NH_2$, $PhC_2H_4NH_2$, $PhC_3H_6NH_2$) with Na^+ differed by up to 200-fold. The introduction of a phenyl group generally weakened the binding, with the benzylamine analogue, $L^3Co_2(PhCH_2NH_2)_4$, showing the lowest affinity. A detailed analysis of the uptake/release rates, k_{in} and k_{out}, revealed that the phenyl-containing derivatives generally exhibited a faster release rate k_{out} and slower uptake rate k_{in}. Since the Na^+-bound species of these phenyl-containing complexes, $L^3Co_2(PhC_nH_{2n}NH_2)_4Na$ (n = 1,2,3), have quite similar structures to each other, in which the Na^+ guest is located at the center of the O_6 cavity, the differences in the binding constants K_a are mainly ascribed to variations in the uptake rates k_{in}. Crystallographic analysis of the guest-free metallohosts, $L^3Co_2(PhC_nH_{2n}NH_2)_4$ (n = 1,2,3), revealed that some of the phenyl and methylene C–H groups interact with the oxygen atoms of the O_6 binding site *via* C–H···O interactions. This suggests that guest binding requires additional energy to overcome this extra stabilization (Fig. 8).[41]

2.4. Ligand exchange of bis(saloph) cobalt(III) metallohosts for control of the guest binding affinity

Since cobalt(III) is inert due to its low-spin d^6 electron configuration, dissociation of the cobalt(III) ion from the tetradentate saloph chelate ligand is essentially negligible. Nevertheless, the Co–N bonds to the monoamine ligands **A** are relatively dynamic, thus allowing the ligand exchange in a site-selective fashion (Fig. 1b). This reactivity is advantageous for

Table 1 Binding constants and uptake/release rate constants for the host–guest complexes of $L^3Co_2\mathbf{A}_4$ with Na^+ [a,b]

	K_a (M^{-1})	k_{in} ($M^{-1}s^{-1}$)	k_{out} (s^{-1})
A = $EtNH_2$	9.6 × 10^6	1.1 × 10^6	0.12
A = $PhCH_2NH_2$	4.9 × 10^4	5.2 × 10^4	1.05
A = $PhC_2H_4NH_2$	3.8 × 10^5	9.0 × 10^4	0.23
A = $PhC_3H_6NH_2$	8.1 × 10^5	1.0 × 10^5	0.12

[a] In CD_3OD. [b] Determined by ^1H NMR spectroscopy. Data taken from ref. 41.

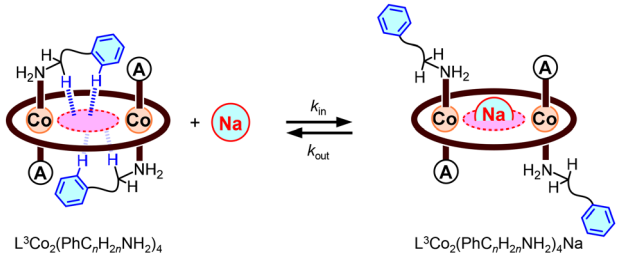

Fig. 8 Guest binding equilibrium of $L^3Co_2(PhC_nH_{2n}NH_2)_4$ (n = 1,2,3). The definitions of the uptake and release kinetic rate constants, k_{in} and k_{out}, for the host–guest binding equilibrium are shown. Extra stabilization *via* C–H···O interactions by the phenyl capping can explain the relatively weaker binding compared to $L^3Co_2(EtNH_2)_4$.

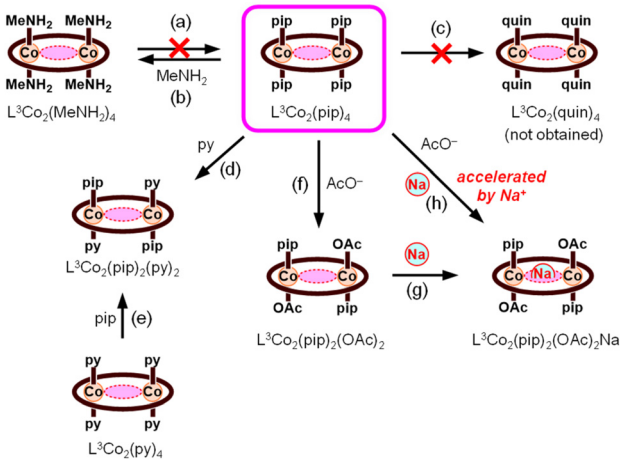

Fig. 9 Structural conversion of $L^3Co_2(pip)_4$ and related complexes *via* ligand exchange. Path (h) represents the acceleration of ligand exchange with AcO^- in the presence of Na^+.

functionalization after the L^3Co_2 dinuclear structures are constructed, *i.e.*, the post-metalation modification enables alteration or fine-tuning of molecular functions, such as the host–guest binding affinity, as seen in the post-synthetic modification of various molecular cages and MOFs.[42] Indeed, the guest binding affinity of the dinuclear metallohosts $L^3Co_2\mathbf{A}_4$ was significantly influenced by the structure of the primary amine ligands **A** introduced at the cobalt(III) centers, as described in the previous section.

In this context, the synthesis of analogous $L^3Co_2\mathbf{A}_4$ complexes bearing different types of amine ligands, such as a secondary amine (pip = piperidine) and a tertiary amine (quin = quinuclidine), was attempted using the same protocol as that for $L^3Co_2(MeNH_2)_4$.[43] Whereas the piperidine-coordinating complex, $L^3Co_2(pip)_4$, was successfully obtained, the quinuclidine-coordinating complex, $L^3Co_2(quin)_4$, was not obtained.

Regarding the ligand exchange reactivity, the methylamine ligands in $L^3Co_2(MeNH_2)_4$ were not readily exchanged with other amines (pip, quin) (Fig. 9a). In contrast, the piperidine-coordinating complex, $L^3Co_2(pip)_4$, was efficiently converted into the methylamine-coordinating complex, $L^3Co_2(MeNH_2)_4$ (Fig. 9b), but not into the quinuclidine complex, $L^3Co_2(quin)_4$ (Fig. 9c). Thus, the affinity order of the amines for the cobalt(III) centers in $L^3Co_2\mathbf{A}_4$ followed the trend of primary amine > secondary amine > tertiary amine, which can be attributed to the steric bulk around the nitrogen donor atom. Among the isolable $L^3Co_2\mathbf{A}_4$ complexes, the piperidine-coordinating complex, $L^3Co_2(pip)_4$, was found to be the best starting complex for ligand exchange, as it exhibited the highest reactivity.[43]

It is noteworthy that the ligand exchange of $L^3Co_2(pip)_4$ with pyridine selectively afforded a di-exchanged product, $L^3Co_2(pip)_2(py)_2$, instead of the tetra-exchanged species, $L^3Co_2(py)_4$ (Fig. 9d). X-ray crystallography and ^1H NMR spectroscopy revealed the anti-diagonal stereoconfiguration of this product, in which each cobalt center bears one pip and one py ligand occupying opposite positions on the two faces, *e.g.*, pip above and py below on one cobalt center, and reverse on the other. This stereoselectivity can be attributed to the doubly curved structure of the L^3Co_2 framework, in which the bulkier piperidine ligands preferentially occupy the two convex faces, while the pyridine ligands reside on the narrower concave faces. The same product, the anti-diagonal $L^3Co_2(pip)_2(py)_2$, was also selectively formed *via* the reverse ligand exchange (py → pip) starting from $L^3Co_2(py)_4$ (Fig. 9e).

A similar anti-diagonal di-exchanged complex, $L^3Co_2(pip)_2(OAc)_2$, was obtained by the reaction of $L^3Co_2(pip)_4$ with acetate ion (Fig. 9f). This complex was obtained as precipitates directly from the reaction mixture in 82% isolated yield.

These results demonstrate that a variety of post-metalation modifications of $L^3Co_2\mathbf{A}_4$ metallohosts can be achieved by exploiting the reactivity of the axial ligands coordinating to the cobalt(III) centers.[43] Such modulations provide a means to tune the binding affinity for cationic guests such as Na^+ within the central O_6 cavity.

The di-exchanged complex, $L^3Co_2(pip)_2(OAc)_2$, showed high affinity for cationic guests, owing to charge compensation of the dicationic L^3Co_2 core by the newly introduced anionic acetato ligands. Indeed, Na^+ ion was quantitatively taken up to form the inclusion complex $L^3Co_2(pip)_2(OAc)_2Na$ (Fig. 9g), whose structure was unambiguously determined by X-ray crystallography.

In contrast, when NaOTf was added to a CD_3CN solution of the starting piperidine-coordinating complex, $L^3Co_2(pip)_4$, formation of the Na^+ inclusion complex was not observed, indicating its lower guest binding affinity. However, upon treatment of this mixture with AcO^-, ligand exchange rapidly proceeded, concomitant with Na^+ uptake, to afford $L^3Co_2(pip)_2(OAc)_2Na$ (Fig. 9h). These observations clearly demonstrate that the guest binding affinity of the piperidine-coordinating complex $L^3Co_2(pip)_4$ is enhanced by exchange of the neutral piperidine ligands with anionic acetato ligands.[43] Moreover, the presence of Na^+ ion significantly enhanced the ligand exchange reactivity of the $L^3Co_2(pip)_4$ metallohost.

Thus, the ligand exchange reactivity and the guest binding affinity of $L^3Co_2(pip)_4$ were mutually enhanced. This interplay became even more evident in the guest binding of $L^3Co_2(pip)_4$ accompanied by exchange with methoxo ligands under solvolytic conditions.

The piperidine-coordinating complex $L^3Co_2(pip)_4$ slowly underwent solvolysis in CD_3OD, affording a new species rather than immediately forming a simple guest-bound complex, $L^3Co_2(pip)_4Na$.[44] Spectroscopic and crystallographic investigations revealed that the resulting product was an inclusion complex $L^3Co_2(pip)_2(OMe)_2Na$, in which two piperidine ligands were replaced by methoxo ligands. Detailed analysis of the reaction progress indicated that the reaction first produced a mono-exchanged guest-bound species, $L^3Co_2(pip)_3(OMe)Na$, which was then converted into the di-exchanged species, $L^3Co_2(pip)_2(OMe)_2Na$. In the first step, ligand exchange and Na^+ uptake appear to occur concurrently.

More precisely, this process can be interpreted in terms of two possible mechanisms. One is the reaction first mechanism (Fig. 10A), in which exchange with the methoxo ligand occurs prior to guest binding. In this mechanism, the coordination of the anionic methoxo ligand cancels the positive charge of the cobalt(III) center, thereby enhancing the binding affinity for cationic guests in the central O_6 cavity. The other is the recognition first mechanism (Fig. 10B), in which guest binding occurs before ligand exchange. In this mechanism, the presence of the guest in the central O_6 cavity facilitates ligand exchange reaction at the cobalt(III) centers.

These two mechanisms can be distinguished by analyzing the ligand exchange kinetics at varying guest concentrations.[45] In practice, the ligand exchange rate of $L^3Co_2(pip)_4$ increased proportionally with the concentration of Na^+, supporting the recognition first mechanism (Fig. 10B). In contrast, the ligand exchange rates observed in the presence of 1 equiv. of K^+ or Rb^+ were not significantly different from that without any guest, supporting the reaction first mechanism (Fig. 10A).[44]

Thus, the mechanism of guest binding can be switched simply by changing the guest ions.

In enzymatic reactions, substrate binding is often accompanied by structural changes in the host protein. The well-known induced-fit mechanism describes a structural change in a protein that occurs as a result of substrate binding. More recently, an alternative mechanism known as conformational selection has been proposed, in which the conformational change precedes substrate binding.[46] The reaction first and recognition first mechanisms proposed in this study correspond to the conformational selection and induced-fit mechanisms, respectively, in enzymatic systems. Notably, this study provides the first demonstration that switching between these two mechanisms can be achieved simply by selecting different guest ions.

2.5. Ligand exchange of bis(saloph) cobalt(III) metallohosts with bridging diamines for guest recognition control

As described in the previous sections, $L^3Co_2(pip)_4$ proved useful as the starting compound for the post-metalation modification to introduce various types of monodentate ligands, particularly primary amines. Its high reactivity toward primary amines also enabled the incorporation of diamine molecules bearing two terminal primary amino groups. Indeed, ligand exchange of $L^3Co_2(pip)_4$ with 1,6-hexanediamine (**DA1**) afforded a doubly bridged metallohost, $L^3Co_2(\mathbf{DA1})_2$, in 77% yield (Fig. 11a). This product has two bridging **DA1** ligands on both faces of the macrocyclic plane.[47]

The utility of the ligand exchange strategy for synthesizing the doubly bridged complex $L^3Co_2(\mathbf{DA1})_2$ was demonstrated by a failed attempt to obtain it directly from its components, H_4L^3, $Co(OAc)_2$, and **DA1**, under aerobic conditions (Fig. 11b). This reaction instead yielded a singly bridged species, formulated as $L^3Co_2H(\mathbf{DA1})_2(OAc)$ (Fig. 11c). These results suggested that the singly bridged species is thermodynamically more favored in the presence of AcO^- than the doubly bridged species. Indeed, the doubly bridged species $L^3Co_2(\mathbf{DA1})_2$ was

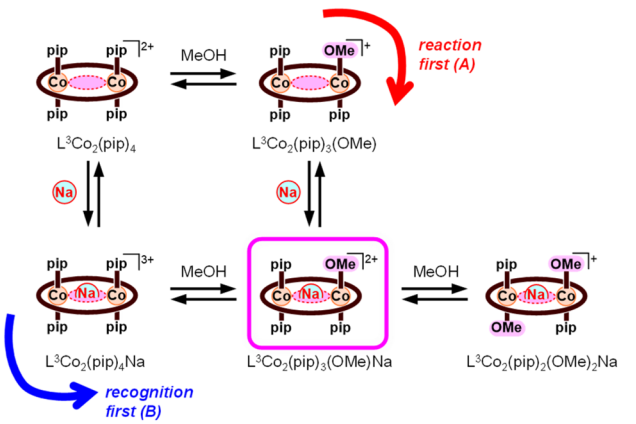

Fig. 10 Guest uptake behavior of $L^3Co_2(pip)_4$ associated with the ligand exchange reaction under solvolytic conditions. The recognition first mechanism (B) is suggested when Na^+ is bound.

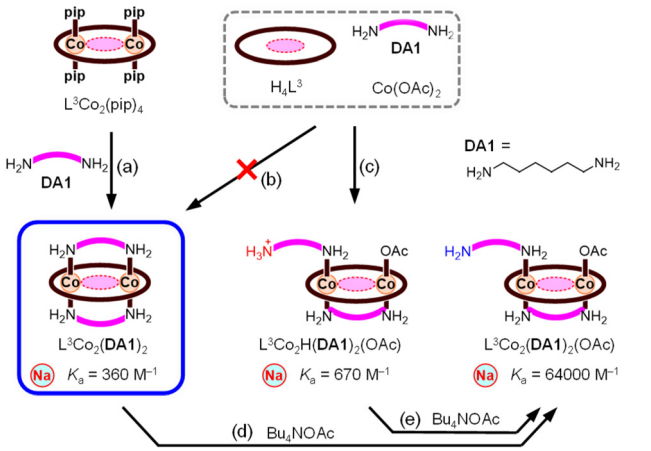

Fig. 11 Formation of doubly and singly bridged metallohosts with the 1,6-hexanediamine ligand (**DA1**) based on the L^3Co_2 macrocycle.

gradually converted into the singly bridged species L^3Co_2(**DA1**)$_2$(OAc) in the presence of AcO^-, although this conversion was slow and incomplete (28% conversion after 24 h) (Fig. 11d).

Among the two types of bridged metallohosts, the doubly bridged species, L^3Co_2(**DA1**)$_2$, showed a lower binding affinity for Na^+ (K_a = 360 M^{-1}), which may be attributed to hindered access of counter anions due to the bridging ligands **DA1**. The Na^+ binding affinity of the singly bridged species, L^3Co_2H(**DA1**)$_2$(OAc), was only slightly higher (K_a = 670 M^{-1}), which can be rationalized by electrostatic repulsion from the protonated amino group (NH_3^+) at the terminus of the non-bridging diamine ligand **DA1**. Indeed, once this complex was deprotonated with Bu_4NOAc (Fig. 11e), the resulting species, L^3Co_2(**DA1**)$_2$(OAc), showed a significantly higher binding affinity for Na^+ (K_a = 64 000 M^{-1}). Thus, the gate-opening from the doubly bridged to the singly bridged structure significantly enhanced guest binding affinity.[47]

As described in the previous sections, the guest binding affinity and ligand exchange reactivity enhanced each other in the case of the piperidine-coordinating complex, $L^3Co_2(pip)_4$. A similar mutual enhancement was observed between the gate-opening reactivity of the doubly bridged species, L^3Co_2(**DA1**)$_2$, and the Na^+ binding in the cavity. While the conversion of the doubly bridged species L^3Co_2(**DA1**)$_2$ into the singly bridged species L^3Co_2(**DA1**)$_2$(OAc) was slow (28% conversion after 24 h; k = 3.7 × 10^{-6} s^{-1}) as mentioned above (Fig. 11d), this reaction was significantly accelerated in the presence of Na^+, by approximately 75-fold (k = 2.8 × 10^{-4} s^{-1}). Thus, the Na^+ binding and the closed → open conversion of the doubly bridged species L^3Co_2(**DA1**)$_2$ proceeded in a mutually promoted manner.[47]

2.6. Shape-complementary introduction of bridging ligands into bis(saloph) cobalt(III) macrocycles

A larger class of macrocyclic bis(saloph) ligands was also employed in the synthesis of dinuclear structures, in which the two bridging ligands connect the cobalt(III) ions.[48] This doubly bridged complex was synthesized by the reaction of macrocycle H_4L^4 (Fig. 2) with $Co(OAc)_2$ followed by the reaction with the bis-pyridine ligand **BP1** (Fig. 12a). The resulting complex, $L^{4a}Co_2$(**BP1**)$_2$ (Fig. 12b), was characterized by NMR spectroscopy and mass spectrometry as well as X-ray crystallography. Given its structural similarity to Pd_2L_4 lantern-shaped cage structures,[49] the doubly bridged dinuclear cobalt(III) complex $L^{4a}Co_2$(**BP1**)$_2$ can be regarded as a *trans*-A_2B_2-type heteroleptic cage, because two types of arms alternately connect the two cobalt(III) ions. Previously, special strategies such as shape-complementary assembly were required for the synthesis of such heteroleptic cages.[50]

Whereas the $L^{4a}Co_2$(**BP1**)$_2$ complex has two identical bridging **BP1** ligands on both faces, two different bridging ligands can also be selectively introduced into the $L^{4a}Co_2$ macrocycle *via* the shape-complementary assembly approach.[51] Indeed, a heteroleptic doubly bridged complex, $L^{4a}Co_2$(**BP2**)(**BP3**), was successfully synthesized (Fig. 12c) using a similar protocol

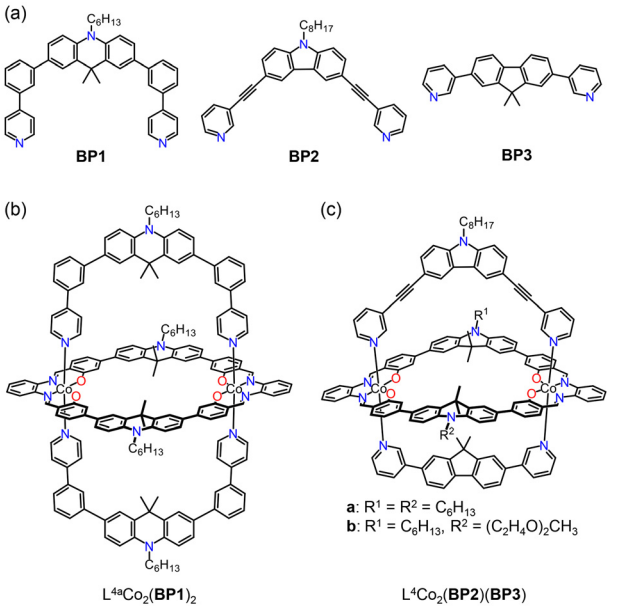

Fig. 12 Lantern-shaped cage structures based on the bis(saloph) macrocycle H_4L^4. (a) Bis(pyridine) ligands used as bridging ligands. (b) Symmetric doubly bridged complex $L^{4a}Co_2$(**BP1**)$_2$. (c) Unsymmetrical doubly bridged complexes L^4Co_2(**BP2**)(**BP3**), which can be regarded as a lantern-shaped cage incorporating three or four different arms.

with a combination of the convergent-shaped **BP2**, which is based on carbazole, and the divergent-shaped **BP3**, which is based on fluorene (Fig. 12a).[48] X-ray crystallography clearly demonstrated the face-selective bridging of the two different bis-pyridine ligands, each geometrically suited to the bent $L^{4a}Co_2$ macrocyclic framework; the divergent-shaped **BP3** binds to the concave face, while the convergent-shaped **BP2** occupies the convex face. Notably, the corresponding reactions using only **BP2** or **BP3** with the $L^{4a}Co_2$ macrocycle failed to yield the doubly bridged structure. Detailed investigation revealed that the selective formation of the mixed-ligand species, $L^{4a}Co_2$(**BP2**)(**BP3**), is ascribed to its thermodynamic stability.

Furthermore, the unsymmetrical macrocycle H_4L^{4b} was employed in the synthesis of the mixed-ligand species $L^{4b}Co_2$(**BP2**)(**BP3**) (Fig. 12c). This complex has four different arms between the two cobalt(III) ions, which can be regarded as an M_2ABCD-type lantern-shaped cage, a structure that was previously considered difficult to synthesize.[48]

3. Functioinalization of tris(saloph) cobalt(III) cages by axial coordination

3.1. Dynamic chirality inversion of helical tris(saloph) cobalt(III) cryptands by ligand exchange

A cryptand-like tris(saloph) cage ligand, H_6L^5 (Fig. 2),[52] features a bicyclic structure in which the three arms are doubly connected through two propeller-shaped triphenylbenzene subunits. Each arm contains a tetradentate H_2saloph chelate coordination site, which can accommodate a transition metal

ion. The triply metalated species, L^5M_3, is also expected to show strong binding affinity toward cationic guest species, due to the negatively polarized phenoxo groups in the [M(saloph)] substructures, as observed in the macrocyclic bis(saloph) analogues L^3M_2. Indeed, the trinuclear nickel(II) complex L^5Ni_3 (Fig. 13a) was found to exhibit unique binding behavior toward alkali metal ions, silver ion, guanidinium ion, *etc.*[52–54]

This cryptand ligand H_6L^5 can be converted into a trinuclear cobalt(III) complex, $L^5Co_3\mathbf{A}_6$. The six axial ligands **A**, coordinating to the three cobalt(III) ions in the saloph arms (Fig. 13b), can be replaced or modified, enabling functionalization and structural conversion of the cryptand framework. In fact, the trinuclear complexes $L^5Co_3\mathbf{A}_6$ (**A** = Me_2NH, pip) were synthesized by the reaction of H_6L^5 with cobalt(II) acetate in the presence of appropriate amines **A** under aerobic conditions.[55]

The three $[Co(saloph)\mathbf{A}_2]^+$ arms of the trinuclear complexes $L^5Co_3\mathbf{A}_6$ form a triple helix that extends toward the two propeller-shaped triphenylbenzene cores at the bridgeheads of the cryptand. In fact, the triple helical structure of the corresponding nickel(II) analogue, L^5Ni_3, was confirmed by X-ray crystallography. This structure exhibits dynamic behavior, enabling interconversion between the *P* and *M* forms.[52,53] The present cobalt(III) analogues $L^5Co_3\mathbf{A}_6$, which contain achiral amine ligands (**A** = Me_2NH, pip), also adopt a similar helical structure. The *P* and *M* forms constitute an enantiomeric pair, yielding an equilibrated racemic mixture due to the dynamic chirality interconversion. However, ligand exchange of the $[Co(saloph)\mathbf{A}_2]^+$ (**A** = Me_2NH, pip) arms with a chiral amine ligand makes the *P* and *M* forms diastereomeric, thereby shifting the *P*/*M* equilibrium accordingly (Fig. 14a).

Indeed, the addition of chiral amines, *S*-**A1** or *S*-**A2**, to $L^5Co_3\mathbf{A}_6$ (**A** = Me_2NH, pip) resulted in ligand exchange with these chiral amines, accompanied by a gradual *P*/*M* equilibrium shift (Fig. 14a).[55] The progress of ligand exchange at the cobalt(III) centers was easily monitored by ^1H NMR spectroscopy as well as mass spectrometry. For example, the dimethylamine-coordinating complex $L^5Co_3(Me_2NH)_6$ was gradually converted to $L^5Co_3(S\text{-}\mathbf{A2})_6$ upon addition of 12 equiv. of the chiral amine *S*-**A2**. This ligand exchange induced an equilibrium shift toward the *P* form, as evidenced by the growth of the negative CD signal at 550 nm (Fig. 15a(ii)). Time-course measurements indicated that the ligand exchange was almost completed within 3 h.

One notable advantage of this system is that the rate of the *P*/*M* equilibrium shift can be modulated by selecting different

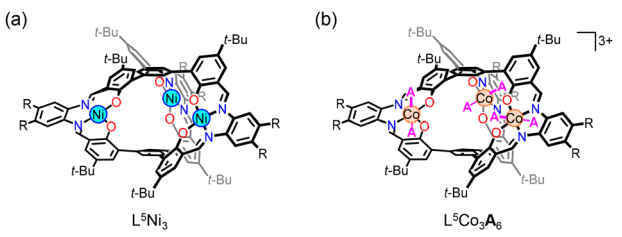

Fig. 13 Chemical structures of the metallocryptands, (a) L^5Ni_3 and (b) $L^5Co_3\mathbf{A}_6$.

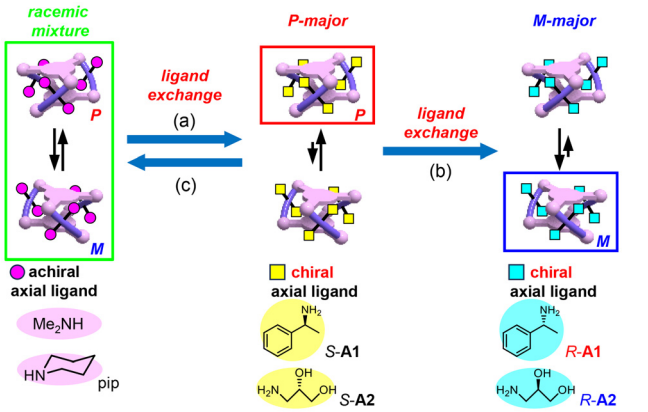

Fig. 14 Control of the *P*/*M* ratio of the helical metallocryptand $L^5Co_3\mathbf{A}_6$ *via* ligand exchange at the cobalt centers.

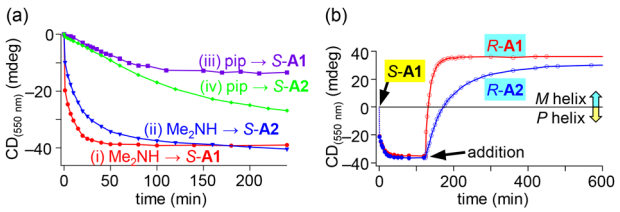

Fig. 15 Time-dependent changes in CD intensity at 550 nm observed during the ligand exchange of $L^5Co_3\mathbf{A}_6$. (a) CD intensity of $L^5Co_3\mathbf{A}_6$ (**A** = Me_2NH, pip) plotted *versus* time after the addition of *S*-**A1** or *S*-**A2** (12 equiv.). (b) CD intensity of $L^5Co_3(Me_2NH)_6$ plotted *versus* time after sequential addition of *S*-**A1** followed by a second chiral amine *R*-**A1** or *R*-**A2** (120 equiv.). Adapted with permission from ref. 55.

combinations of the initial achiral amine **A** and the added chiral amine (Fig. 15a(i–iv)). For example, when the chiral amine *S*-**A1** was added instead of *S*-**A2** to $L^5Co_3(Me_2NH)_6$, the equilibrium shift proceeded more rapidly. In contrast, when the piperidine-coordinating complex $L^5Co_3(pip)_6$ was used instead of $L^5Co_3(Me_2NH)_6$ as the initial complex, the reaction became significantly slower. As a result, among the four possible combinations, the rate of the *P*/*M* equilibrium shift differed by up to 60-fold.[55]

The ligand exchange strategy was also effective in inducing *P*/*M* chirality inversion when chiral amines with the opposite stereoconfigurations were used as the initial and added chiral sources (Fig. 14b). In fact, a *P*-major mixture was first prepared by the addition of the chiral amine *S*-**A1** to racemic $L^5Co_3(Me_2NH)_6$, which was then inverted to an *M*-favored mixture upon addition of a large excess of another chiral amine, *R*-**A1**, possessing the opposite stereoconfiguration. This *P*/*M* chirality inversion was monitored by time-dependent CD spectroscopy (Fig. 15b); upon addition of the second amine, the negative CD signal at 550 nm decreased and inverted within 8 min, then became nearly constant after 1 h. When another second chiral amine, *R*-**A2**, was used instead of *R*-**A1**, the $P \rightarrow M$ chirality inversion occurred 6 times more slowly. Thus, the $L^5Co_3\mathbf{A}_6$ complex was shown to be a useful helical

molecular platform[56,57] capable of modulating the response speeds of both the *P*/*M* equilibrium shifts and the chirality inversion through the choice of initial and added amines.[55]

The reverse ligand exchange, *i.e.*, replacing a chiral ligand with an achiral ligand, showed a unique time-dependent change. When the achiral amine, piperidine, was added to $L^5Co_3(S\text{-}\mathbf{A1})_6$, the six chiral amine ligands (*S*-**A1**) were gradually replaced by piperidine, yielding $L^5Co_3(pip)_6$, which no longer contained any chiral sources in its molecular structure. This process converted a diastereomeric pair of $L^5Co_3(S\text{-}\mathbf{A1})_6$ with a biased *P*/*M* ratio (*P*/*M* = 88 : 12) into an enantiomeric pair, which, in principle, could afford a racemic *P*/*M* mixture (Fig. 14c), assuming rapid *P*/*M* interconversion. Thus, the CD signal was expected to monotonically decrease and eventually become silent along the progress of the ligand exchange. However, the CD intensity exhibited an unusual irregular time-dependent change beyond expectations.[58]

As already stated, $L^5Co_3(S\text{-}\mathbf{A1})_6$ exhibited a negative CD signal at 550 nm due to its *P*-preference (Fig. 16a(i)), but the addition of a large excess of piperidine as an achiral amine (120 equiv.) caused an immediate decrease in the CD signal followed by a reversal instead of a simple monotonic decay to zero. The resulting positive signal reached its maximum intensity after 2 h (Fig. 16a(ii)), and then gradually diminished, eventually becoming CD-silent after 3 d (Fig. 16b(i, ii) and c). This behavior indicated that the predominant chirality transiently shifted from *P* to *M* before complete racemization occurred (Fig. 17).[58] Normally, when an optically active chiral compound undergoes racemization, its optical purity monotonically decreases to zero, and the chirality never inverts during the racemization process. Such a sign inversion before reaching equilibrium position is commonly observed in physical phenomena, such as damped oscillations, but is quite rare in the relaxation behavior of chemical reactions.

This unusual and irregular time-course change during the racemization of $L^5Co_3(S\text{-}\mathbf{A1})_6$ was investigated in detail by spectroscopic techniques, which clearly demonstrated that the six-step ligand exchange with piperidine was completed within 1 h to afford $L^5Co_3(pip)_6$, *i.e.*, at an early stage of the entire time-dependent process. The rate constants for all the ligand exchange steps were determined, revealing that the tetra-exchanged intermediate, $L^5Co_3(S\text{-}\mathbf{A1})_2(pip)_4$, which still retained two chiral *S*-**A1** ligands, preferred the reversed stereoconfiguration, namely the *M* helix (Fig. 17a). It then lost all the chiral *S*-**A1** ligands while maintaining this *M*-biased configuration to afford $L^5Co_3(pip)_6$ (Fig. 17b), which could undergo only slow racemization over 2–3 d (Fig. 17c) due to the steric hindrance imposed by the six bulky piperidine ligands.[58]

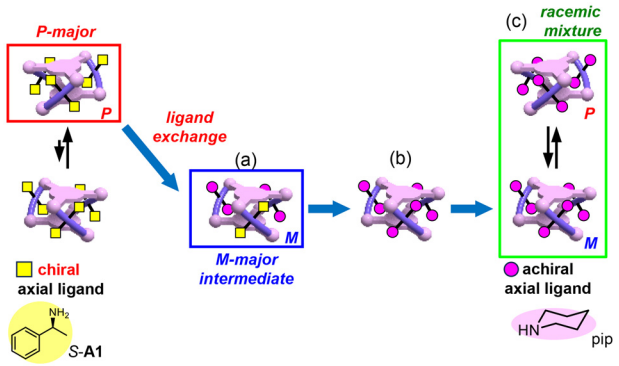

Fig. 17 Overview of the transient *P*/*M* chirality inversion observed during the racemization of $L^5Co_3(S\text{-}\mathbf{A1})_6$ *via* ligand exchange with piperidine.

Considering the above findings, opposite chiralities emerged during the forward (achiral → chiral; Fig. 14a) and reverse (chiral → achiral; Fig. 14c) ligand exchange reactions between piperidine and the chiral amine *S*-**A1**. During the ligand exchange of $L^5Co_3(pip)_6$ with *S*-**A1**, the *P* form was always dominant (Fig. 14a), resulting in a monotonic increase in the *P*/*M* ratio. In contrast, the *M* form transiently became dominant during the ligand exchange of $L^5Co_3(S\text{-}\mathbf{A1})_6$ with piperidine (Fig. 14c), leading to an unexpected transient chirality inversion (Fig. 17). This behavior constitutes a hysteretic cycle, because the *M* form appeared only in the reverse reaction. Such an unusual time-dependent change was discovered primarily because both the multistep ligand exchange at the cobalt(III) centers and the *P*/*M* chirality inversion of the $L^5Co_3\mathbf{A}_6$ framework occurred on a similar timescale of minutes to hours, readily observable on a human time scale.

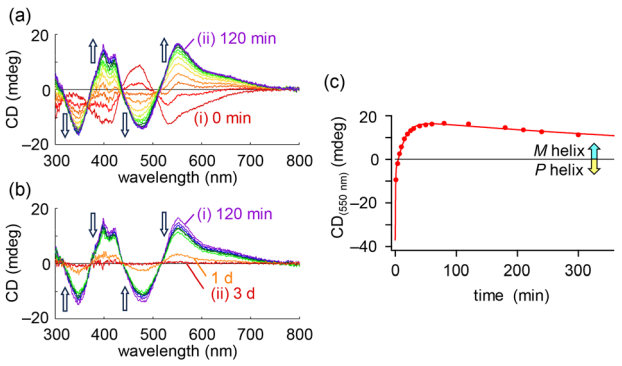

Fig. 16 Time-dependent changes in the CD spectra of metallocryptand $L^5Co_3(S\text{-}\mathbf{A1})_6$ after addition of piperidine (120 equiv.). (a) Full CD spectra for 0–120 min and (b) after 120 min. (c) CD intensity at 550 nm plotted *versus* time. Adapted with permission from ref. 58.

3.2. Tris(saloph) cobalt(III) closed cages for guest uptake/release control

Closed-cage type host molecules were anticipated to be formed when diamine ligands were introduced into the cryptand cage L^5Co_3 in a bridging fashion between neighboring cobalt(III) ions at the cage apertures, as demonstrated in the macrocyclic dinuclear complex $L^3Co_2(\mathbf{DA1})_2$. The resulting closed cage species, $L^5Co_3(diamine)_3$ (Fig. 18), could serve as a molecular container, because guest uptake/release is completely blocked by the bridging diamine

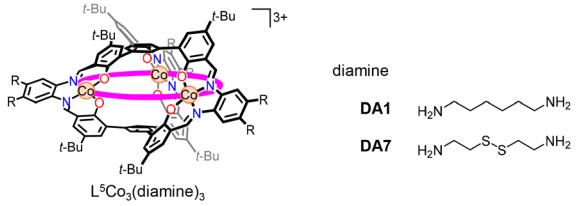

Fig. 18 Chemical structures of closed metallocryptands, $L^5Co_3(diamine)_3$.

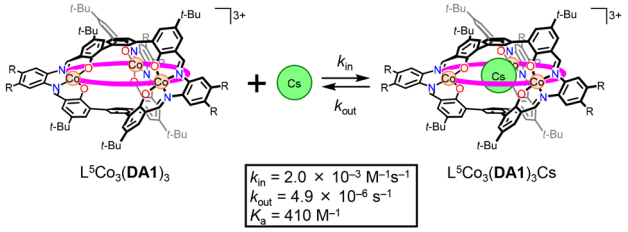

Fig. 20 Slow uptake of Cs^+ by closed metallocryptand $L^5Co_3(\mathbf{DA1})_3$.

ligands, functioning much like a container with a cap or a lid. This effective gating arises from the kinetic inertness of the cobalt(III) centers, whose slow Co–N bond cleavage/formation even suppresses transient formation of open intermediates that could allow guest entry/exit. In contrast, the corresponding monoamine-coordinating analogue, $L^5Co_3\mathbf{A}_6$ (Fig. 13b), would behave as an open container, which allows rapid guest entry/exit. Thus, interconversion between the open and closed forms functions analogously to opening and closing a container lid,[59,60] providing control over the uptake and release of molecular and ionic guests.

The triply bridged closed metallohost, $L^5Co_3(\mathbf{DA1})_3$, was synthesized by the reaction of the cryptand ligand H_6L^5 with cobalt(II) acetate in the presence of diamine **DA1** under aerobic conditions.[61] This complex was also accessible *via* ligand exchange of the methylamine-coordinating open-cage complex, $L^5Co_3(MeNH_2)_6$, with the diamine **DA1**. X-ray crystallography clearly revealed the triply bridged structure of this $L^5Co_3(\mathbf{DA1})_3$, in which three **DA1** molecules connect neighboring cobalt(III) ions to form a cyclic framework. These three diamine molecules are well accommodated in the grooves of the L^5Co_3 triple helix, nearly completely sealing the apertures (Fig. 19a). Nevertheless, sufficient space remains at the center of the $L^5Co_3(\mathbf{DA1})_3$ cryptand to accommodate a guest species.

As expected, the bridging ligands effectively blocked the uptake of guest species such as alkali metal ions into the cavity of $L^5Co_3(\mathbf{DA1})_3$, as evidenced by the ^1H NMR spectra recorded immediately after guest addition. Notably, larger alkali metal ions such as Cs^+ and Rb^+ were taken up only very slowly, requiring approximately 5 d to reach equilibrium (Fig. 19b). This indicates that the guest uptake was kinetically suppressed, rather than thermodynamically unfavorable, and

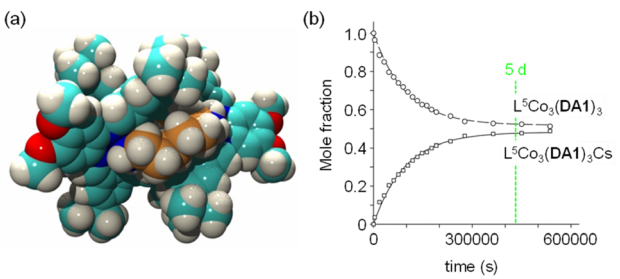

Fig. 19 (a) X-ray crystal structure of $L^5Co_3(\mathbf{DA1})_3$. (b) Guest uptake kinetics of $L^5Co_3(\mathbf{DA1})_3$ in CD_3OD. Adapted with permission from ref. 61.

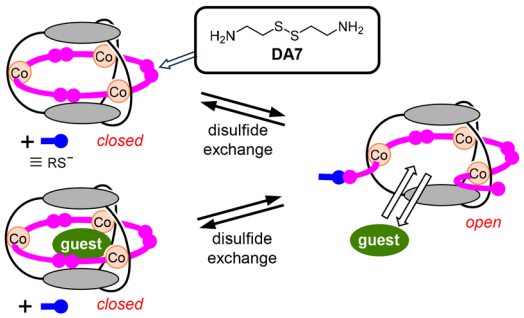

Fig. 21 Proposed mechanism for guest uptake by $L^5Co_3(\mathbf{DA7})_3$ *via* disulfide exchange accelerated by a thiolate ion.

that the closed cage $L^5Co_3(\mathbf{DA1})_3$ retained its intrinsic affinity for guest binding. Kinetic analysis revealed that guest uptake into the closed cage $L^5Co_3(\mathbf{DA1})_3$ proceeded at least 2000 times more slowly than into the corresponding open cage $L^5Co_3(MeNH_2)_6$ (Fig. 20).[61]

A related closed-cage metallocryptand, $L^5Co_3(\mathbf{DA7})_3$, bearing cystamine bridging ligands **DA7**, was also synthesized (Fig. 18).[62] This **DA7** ligand contains a disulfide bond, which is known to behave dynamically in the presence of nucleophiles[63] and to remain static in their absence. Indeed, the presence of a thiolate anion was found to accelerate Cs^+ uptake into $L^5Co_3(\mathbf{DA7})_3$ by a factor of 14, whereas in its absence, the bridging **DA7** ligands effectively blocked Cs^+ uptake, as observed for the hexanediamine analogue, $L^5Co_3(\mathbf{DA1})_3$.

The presence of the thiolate anion promoted the disulfide exchange equilibrium, transiently generating an open-cage intermediate that allows rapid guest entry/exit through the apertures (Fig. 21). In this system, the apertures of the L^5Co_3 cage were initially sealed by the introduction of bridging ligands through coordination bond formation, thereby suppressing guest uptake/release. These apertures were then transiently opened in the presence of a nucleophile *via* disulfide exchange reactions.

4. Conclusions

Various types of cobalt(III) complexes bearing bis- and tris(saloph) ligands have been synthesized and shown to

exhibit dynamic behaviors, despite the typically inert low-spin d^6 electron configuration of cobalt(III) centers. This dynamic character arises primarily from the selective exchangeability of the two axial monodentate ligands in the $[Co(saloph)X_2]^+$ units with ligands such as primary amines, pyridine, and anionic species. Such ligand exchange enables the functionalization and dynamic switching of multi-metallic structures, including reversible redox-driven dissociation/reassociation, modulation of host–guest binding affinity and kinetics, chirality control with time-dependent inversion, and gating of guest uptake through cage closure.

In some systems, guest binding also influences ligand exchange kinetics, expanding the functional scope of these coordination platforms. Thus, the controlled introduction, removal, and exchange of axial ligands has proven to be a powerful strategy for creating functional and responsive metallohosts and metallo-supramolecular systems.

At the same time, several challenges and limitations remain to be addressed. For example, the long-term stability of axial ligands under various conditions, the potential fatigue of the systems under repeated switching cycles, and limitations in guest selectivity are all important issues that require further investigation. Understanding and overcoming these challenges will be essential for translating these dynamic systems into practical stimuli-responsive materials and molecular devices.

Conflicts of interest

There are no conflicts to declare.

Data availability

Data sharing is not applicable to this article as no new data were created or analyzed in this study.

Acknowledgements

The author warmly thanks all coworkers, collaborators, and past and present group members for their contributions to the work carried out in his laboratory. Special thanks are due to Prof. Yoko Sakata (Nagoya University), Dr Naoki Ousaka (Kyushu University), and Dr Sk Asif Ikbal (Kanazawa University) for their dedicated contributions, and to Prof. Tatsuya Nabeshima (University of Tsukuba) for valuable advice and discussions. The research cited in this article was supported by the Japan Society for the Promotion of Science (KAKENHI Grants JP21H05477 and JP23H04021 [Condensed Conjugation] as well as JP16H06510 [Coordination Asymmetry], JP18H03913, JP20K21206, JP23H01972, and JP23K17928), the CHOZEN Project at Kanazawa University, and the World Premier International Research Center Initiative (WPI), MEXT, Japan.

References

1 (*a*) P. Pfeiffer, E. Breith, E. Lübbe and T. Tsumaki, *Liebigs Ann. Chem.*, 1933, **503**, 84–130; (*b*) P. Pfeiffer, T. Hesse, H. Pfitzner, W. Scholl and H. Thielert, *J. Prakt. Chem.*, 1937, **149**, 217–296; (*c*) C. S. Marvel, S. A. Aspey and E. A. Dudley, *J. Am. Chem. Soc.*, 1956, **78**, 4905–4909.

2 (*a*) E. N. Jacobsen, Asymmetric Catalytic Epoxidation of Unfunctionalized Olefins in *Catalytic Asymmetric Synthesis*, ed. I. Ojima, VCH, New York, 1993, ch. 4.2, pp. 159–202; (*b*) T. Katsuki, *Coord. Chem. Rev.*, 1995, **140**, 189–214; (*c*) E. N. Jacobsen, *Acc. Chem. Res.*, 2000, **33**, 421–431.

3 N. Hoshino, *Coord. Chem. Rev.*, 1998, **174**, 77–108.

4 (*a*) G. Consiglio, I. P. Oliveri, S. Failla and S. di Bella, *Molecules*, 2019, **24**, 2514; (*b*) S. di Bella, *Dalton Trans.*, 2021, **50**, 6050–6063.

5 H. Miyasaka, A. Saitoh and S. Abe, *Coord. Chem. Rev.*, 2007, **251**, 2622–2664.

6 (*a*) X. Yang, R. A. Jones and S. Huang, *Coord. Chem. Rev.*, 2014, **273–274**, 63–75; (*b*) S. di Bella and I. Fragalà, *Synth. Met.*, 2000, **115**, 191–196; (*c*) P. G. Lacroix, *Eur. J. Inorg. Chem.*, 2001, 339–348.

7 (*a*) H.-Y. Yin, J. Tang and J.-L. Zhang, *Eur. J. Inorg. Chem.*, 2017, 5085–5093; (*b*) A. Erxleben, *Inorg. Chim. Acta*, 2018, **472**, 40–57; (*c*) L. A. Alfonso-Herrera, D. Hernández-Romero, J. A. Cruz-Navarro, Á. Ramos-Ligonio, A. López-Monteon, J. M. Rivera-Villanueva, D. Morales-Morales and R. Colorado-Peralta, *Coord. Chem. Rev.*, 2024, **505**, 215698.

8 (*a*) M. J. MacLachlan, *Pure Appl. Chem.*, 2006, **78**, 873–888; (*b*) A. W. Kleij, *Chem. – Eur. J.*, 2008, **14**, 10520–10529; (*c*) A. W. Kleij, *Eur. J. Inorg. Chem.*, 2009, 193–205; (*d*) T. Glaser, *Chem. Commun.*, 2011, **47**, 116–130; (*e*) C. J. Whiteoak, G. Salassa and A. W. Kleij, *Chem. Soc. Rev.*, 2012, **41**, 622–631.

9 (*a*) T. Nabeshima and S. Akine, *Chem. Rec.*, 2008, **8**, 240–251; (*b*) S. Akine and T. Nabeshima, *Dalton Trans.*, 2009, 10395–10408; (*c*) T. Nabeshima, S. Akine, C. Ikeda and M. Yamamura, *Chem. Lett.*, 2010, **39**, 10–16; (*d*) S. Akine, *J. Inclusion Phenom. Macrocyclic Chem.*, 2012, **72**, 25–54; (*e*) S. Akine, Metal Complexes with Oligo(salen)-Type Ligands in *The Chemistry of Metal Phenolates*, ed. J. Zabicky, Patai's Chemistry of Functional Groups, John Wiley & Sons Ltd, Chichester, 2018, ch. 4, vol. 2, pp. 153–194; (*f*) M. T. Chaudhry, S. Akine and M. J. MacLachlan, *Chem. Soc. Rev.*, 2021, **50**, 10713–10732.

10 (*a*) S. J. Wezenberg and A. W. Kleij, *Angew. Chem., Int. Ed.*, 2008, **47**, 2354–2364; (*b*) S. M. Elbert and M. Mastalerz, *Org. Mater.*, 2020, **2**, 182–203.

11 (*a*) R. M. Haak, S. J. Wezenberg and A. W. Kleij, *Chem. Commun.*, 2010, **46**, 2713–2723; (*b*) A. Decortes, A. M. Castilla and A. W. Kleij, *Angew. Chem., Int. Ed.*, 2010, **49**, 9822–9837; (*c*) D. E. White, P. M. Tadross, Z. Lu and E. N. Jacobsen, *Tetrahedron*, 2014, **70**, 4165–4180.

12 For acyclic salen/saloph oligomers, see: (*a*) J. H. Chong, S. J. Ardakani, K. J. Smith and M. J. MacLachlan, *Chem. – Eur. J.*, 2009, **15**, 11824–11828; (*b*) S. J. Wezenberg,

G. Salassa, E. C. Escudero-Adán, J. Benet-Buchholz and A. W. Kleij, *Angew. Chem., Int. Ed.*, 2011, **50**, 713–716; (*c*) T. J. Dunn, C. F. Ramogida, C. Simmonds, A. Paterson, E. W. Y. Wong, L. Chiang, Y. Shimazaki and T. Storr, *Inorg. Chem.*, 2011, **50**, 6746–6755; (*d*) M. Mastalerz and I. M. Oppel, *Eur. J. Org. Chem.*, 2011, 5971–5980; (*e*) T. J. Dunn, L. Chiang, C. F. Ramogida, M. I. Webb, D. Savard, M. Sakaguchi, T. Ogura, Y. Shimazaki and T. Storr, *Dalton Trans.*, 2012, **41**, 7905–7914; (*f*) H. Achira, M. Ito, T. Mutai, I. Yoshikawa, K. Araki and H. Houjou, *Dalton Trans.*, 2014, **43**, 5899–5907; (*g*) S. A. Ikbal, Y. Sakata and S. Akine, *Dalton Trans.*, 2021, **50**, 4119–4123.

13 (*a*) M. E. Briggs and A. I. Cooper, *Chem. Mater.*, 2017, **29**, 149–157; (*b*) M. Mastalerz, *Acc. Chem. Res.*, 2018, **51**, 2411–2422.

14 (*a*) S. J. Rowan, S. J. Cantrill, G. R. L. Cousins, J. K. M. Sanders and J. F. Stoddart, *Angew. Chem., Int. Ed.*, 2002, **41**, 898–952; (*b*) M. Mastalerz, *Angew. Chem., Int. Ed.*, 2010, **49**, 5042–5053; (*c*) Y. Jin, C. Yu, R. J. Denman and W. Zhang, *Chem. Soc. Rev.*, 2013, **42**, 6634–6654.

15 (*a*) A. G. Manfredotti and C. Guastini, *Acta Crystallogr., Sect. C: Cryst. Struct. Commun.*, 1983, **C39**, 863–865; (*b*) A. Radha, M. Seshasayee, K. Ramalingam and G. Aravamudan, *Acta Crystallogr., Sect. C: Cryst. Struct. Commun.*, 1985, **41**, 1169–1171; (*c*) J. Wang, F.-L. Bei, X.-Y. Xu, X.-J. Yang and X. Wang, *J. Chem. Crystallogr.*, 2003, **33**, 845–849.

16 (*a*) G. D. Fallon and B. M. Gatehouse, *Acta Crystallogr., Sect. B*, 1976, **32**, 2591–2597; (*b*) N. Kumari, R. Prajapati and L. Mishra, *Polyhedron*, 2008, **27**, 241–248; (*c*) S. Mahato, P. Rawal, A. K. Devadkar, M. Joshi, A. R. Choudhury, B. Biswas, P. Gupta and T. K. Panda, *Org. Biomol. Chem.*, 2022, **20**, 1103–1111; (*d*) Y. Sekine, S. Kusumoto, A. Sugimoto, M. Nakaya and S. Hayami, *Cryst. Growth Des.*, 2023, **23**, 2013–2017.

17 (*a*) D. Hall and F. H. Moore, *J. Chem. Soc. A*, 1966, 1822–1824; (*b*) C. A. Barboza, J. C. Germino, A. M. Santana, F. J. Quites, P. A. M. Vazquez and T. D. Z. Atvars, *J. Phys. Chem. C*, 2015, **119**, 6152–6163.

18 (*a*) J. Reglinski, S. Morris and D. E. Stevenson, *Polyhedron*, 2002, **21**, 2175–2182; (*b*) J. S. Matalobos, A. M. García-Deibe, M. Fondo, D. Navarro and M. R. Bermejo, *Inorg. Chem. Commun.*, 2004, **7**, 311–314; (*c*) A. W. Kleij, M. Kuil, M. Lutz, D. M. Tooke, A. L. Spek, P. C. J. Kamer, P. W. N. M. van Leeuwen and J. N. H. Reek, *Inorg. Chim. Acta*, 2006, **359**, 1807–1814; (*d*) M. Odoko, N. Tsuchida and N. Okabe, *Acta Crystallogr., Sect. E: Struct. Rep. Online*, 2006, **E62**, m708–m709.

19 For a review, see: A. W. Kleij, *Dalton Trans.*, 2009, 4635–4639.

20 (*a*) A. W. Kleij, M. Kuil, D. M. Tooke, M. Lutz, A. L. Spek and J. N. H. Reek, *Chem. – Eur. J.*, 2005, **11**, 4743–4750; (*b*) M. Kuil, P. E. Goudriaan, P. W. N. M. van Leeuwen and J. N. H. Reek, *Chem. Commun.*, 2006, 4679–4681; (*c*) M. Kuil, I. M. Puijk, A. W. Kleij, D. M. Tooke, A. L. Spek and J. N. H. Reek, *Chem. – Asian J.*, 2009, **4**, 50–57; (*d*) M. Kuil, P. E. Goudriaan, A. W. Kleij, D. M. Tooke, A. L. Spek, P. W. N. M. van Leeuwen and J. N. H. Reek, *Dalton Trans.*, 2007, 2311–2320; (*e*) T. Gadzikwa, R. Bellini, H. L. Dekker and J. N. H. Reek, *J. Am. Chem. Soc.*, 2012, **134**, 2860–2863.

21 (*a*) A. W. Kleij, M. Kuil, D. M. Tooke, A. L. Spek and J. N. H. Reek, *Inorg. Chem.*, 2007, **46**, 5829–5831; (*b*) J. Flapper and J. N. H. Reek, *Angew. Chem., Int. Ed.*, 2007, **46**, 8590–8592; (*c*) G. Salassa, A. M. Castilla and A. W. Kleij, *Dalton Trans.*, 2011, **40**, 5236–5243; (*d*) I. Jacobs, A. C. T. van Duin, A. W. Kleij, M. Kuil, D. M. Tooke, A. L. Spek and J. N. H. Reek, *Catal. Sci. Technol.*, 2013, **3**, 1955–1963; (*e*) D. Anselmo, R. Gramage-Doria, T. Besset, M. V. Escárcega-Bobadilla, G. Salassa, E. C. Escudero-Adán, M. M. Belmonte, E. Martin, J. N. H. Reek and A. W. Kleij, *Dalton Trans.*, 2013, **42**, 7595–7603.

22 M. Karmakar and S. Chattopadhyay, *J. Mol. Struct.*, 2019, **1186**, 155–186.

23 (*a*) M. Amirnasr, K. J. Schenk, A. Gorji and R. Vafazadeh, *Polyhedron*, 2001, **20**, 695–702; (*b*) M. Salehi, S. Meghdadi, M. Amirnasr and K. Mereiter, *Acta Crystallogr., Sect. E: Struct. Rep. Online*, 2009, **65**, m942–m943.

24 Ruthenium complex was also used as a platform of functionalization, see: K. Chichak, U. Jacquemard and N. R. Branda, *Eur. J. Inorg. Chem.*, 2002, 357–368.

25 (*a*) S. C. F. Au-Yeung and D. R. Eaton, *Inorg. Chem.*, 1984, **23**, 1517–1520; (*b*) M. F. Summers, L. G. Marzilli, N. Bresciani-Pahor and L. Randaccio, *J. Am. Chem. Soc.*, 1984, **106**, 4478–4485; (*c*) L. M. Manus, R. J. Holbrook, T. A. Atesin, M. C. Heffern, A. S. Harney, A. L. Eckermann and T. J. Meade, *Inorg. Chem.*, 2013, **52**, 1069–1076.

26 S. Akine, *Dalton Trans.*, 2021, **50**, 4429–4444.

27 (*a*) E. Eichhorn, A. Rieker, B. Speiser and H. Stahl, *Inorg. Chem.*, 1997, **36**, 3307–3317; (*b*) A. A. Khandar, B. Shaabani, F. Belaj and A. Bakhtiari, *Inorg. Chim. Acta*, 2007, **360**, 3255–3264.

28 (*a*) M. J. Hardie and C. L. Raston, *Angew. Chem., Int. Ed.*, 2000, **39**, 3835–3839; (*b*) D. A. Leigh, P. J. Lusby, R. T. McBurney, A. Morelli, A. M. Z. Slawin, A. R. Thomson and D. B. Walker, *J. Am. Chem. Soc.*, 2009, **131**, 3762–3771; (*c*) T. Nishino, Y. Yamada, S. Akine, K. Sugimoto and K. Tanaka, *Dalton Trans.*, 2016, **45**, 3831–3837; (*d*) Y.-L. Lu, K. Wu, Y.-H. Huang, W.-C. Li, Z.-M. Cao, X.-H. Yan, X.-D. Zhang, C.-H. Liu, J. Ruan, H.-S. Xu, M. Pan and C.-Y. Su, *J. Am. Chem. Soc.*, 2024, **146**, 20414–20424.

29 H. Shimakoshi, H. Takemoto, I. Aritome and Y. Hisaeda, *Tetrahedron Lett.*, 2002, **43**, 4809–4812.

30 H. Shimakoshi, T. Takemoto, I. Aritome and Y. Hisaeda, *Inorg. Chem.*, 2005, **44**, 9134–9136.

31 H. Shimakoshi, S. Hirose, M. Ohba, T. Shiga, H. Ōkawa and Y. Hisaeda, *Bull. Chem. Soc. Jpn.*, 2005, **78**, 1040–1046.

32 H. Shimakoshi, K. Shibata and Y. Hisaeda, *Inorg. Chem.*, 2009, **48**, 1045–1052.

33 H. Shimakoshi and Y. Hisaeda, *J. Synth. Org. Chem., Jpn.*, 2012, **70**, 60–70.

34 (*a*) S. Akine, F. Utsuno and T. Nabeshima, *Chem. Commun.*, 2010, **46**, 1029–1031; (*b*) S. Akine, F. Utsuno, S. Piao,

H. Orita, S. Tsuzuki and T. Nabeshima, *Inorg. Chem.*, 2016, **55**, 810–821.

35 (*a*) M. Cametti, Y. Sakata, J. Martí-Rujas and S. Akine, *Inorg. Chem.*, 2019, **58**, 14871–14875; (*b*) M. T. Chaudhry, B. O. Patrick, S. Akine and M. J. MacLachlan, *Org. Biomol. Chem.*, 2022, **20**, 8259–8268; (*c*) S. Akine, M. Nakano, Y. Sakata and S. Yano, *Chem. – Eur. J.*, 2024, **30**, e202403071.

36 For related macrocyclic bis(saloph) hosts with different sizes, see: (*a*) F. C. J. M. van Veggel, M. Bos, S. Harkema, W. Verboom and D. N. Reinhoudt, *Angew. Chem., Int. Ed. Engl.*, 1989, **28**, 746–748; (*b*) F. C. J. M. van Veggel, M. Bos, S. Harkema, H. van de Bovenkamp, W. Verboom, J. Reedijk and D. N. Reinhoudt, *J. Org. Chem.*, 1991, **56**, 225–235; (*c*) Y. Sakata, S. Kobayashi and S. Akine, *Chem. Commun.*, 2017, **53**, 6363–6366; (*d*) Y. Sakata, S. Kobayashi, M. Yamamoto, K. Doken, M. Kamezawa, S. Yamaki and S. Akine, *Commun. Chem.*, 2024, **7**, 166; (*e*) S. Akine, Z. Varadi and T. Nabeshima, *Eur. J. Inorg. Chem.*, 2013, 5987–5998.

37 For representative macrocyclic tris(saloph) hosts, see: (*a*) S. Akine, T. Taniguchi and T. Nabeshima, *Tetrahedron Lett.*, 2001, **42**, 8861–8864; (*b*) A. J. Gallant and M. J. MacLachlan, *Angew. Chem., Int. Ed.*, 2003, **42**, 5307–5310; (*c*) S. Akine, D. Hashimoto, T. Saiki and T. Nabeshima, *Tetrahedron Lett.*, 2004, **45**, 4225–4227; (*d*) T. Nabeshima, H. Miyazaki, A. Iwasaki, S. Akine, T. Saiki, C. Ikeda and S. Sato, *Chem. Lett.*, 2006, **35**, 1070–1071; (*e*) S. Akine, S. Sunaga, T. Taniguchi, H. Miyazaki and T. Nabeshima, *Inorg. Chem.*, 2007, **46**, 2959–2961; (*f*) A. Yamashita, A. Watanabe, S. Akine, T. Nabeshima, M. Nakano, T. Yamamura and T. Kajiwara, *Angew. Chem., Int. Ed.*, 2011, **50**, 4016–4019; (*g*) S. Akine, S. Sunaga and T. Nabeshima, *Chem. – Eur. J.*, 2011, **17**, 6853–6861; (*h*) T. Nakamura, S. Yano, Y.-F. Liu and T. Nabeshima, *Inorg. Chem.*, 2024, **63**, 12697–12702.

38 For related macrocyclic tetrakis(saloph) hosts, see: (*a*) S.-S. Sun, C. L. Stern, S. T. Nguyen and J. T. Hupp, *J. Am. Chem. Soc.*, 2004, **126**, 6314–6326; (*b*) S.-i. Kawano, Y. Ishida and K. Tanaka, *J. Am. Chem. Soc.*, 2015, **137**, 2295–2302; (*c*) T. Nakamura, S. Tsukuda and T. Nabeshima, *J. Am. Chem. Soc.*, 2019, **141**, 6462–6467; (*d*) S.-i. Kawano, M. Nakaya, M. Saitow, A. Ishiguro, T. Yanai, J. Onoe and K. Tanaka, *J. Am. Chem. Soc.*, 2022, **144**, 6749–6758.

39 Y. Sakata, C. Murata and S. Akine, *Nat. Commun.*, 2017, **8**, 16005.

40 (*a*) C. Marquez and W. M. Nau, *Angew. Chem., Int. Ed.*, 2001, **40**, 3155–3160; (*b*) O. Danylyuk, V. P. Fedin and V. Sashuk, *Chem. Commun.*, 2013, **49**, 1859–1861.

41 D. Walter, Y. Sakata and S. Akine, *Chem. – Asian J.*, 2025, **20**, e202401876.

42 (*a*) D. A. Roberts, B. S. Pilgrim and J. R. Nitschke, *Chem. Soc. Rev.*, 2018, **47**, 626–644; (*b*) M.-M. Gan, J.-Q. Liu, L. Zhang, Y.-Y. Wang, F. E. Hahn and Y.-F. Han, *Chem. Rev.*, 2018, **118**, 9587–9641.

43 Y. Sakata, M. Okada, M. Tamiya and S. Akine, *Chem. – Eur. J.*, 2020, **26**, 7595–7601.

44 Y. Sakata, M. Tamiya, M. Okada and S. Akine, *J. Am. Chem. Soc.*, 2019, **141**, 15597–15604.

45 (*a*) P. J. Tummino and R. A. Copeland, *Biochemistry*, 2008, **47**, 5481–5492; (*b*) G. G. Hammes, Y.-C. Chang and T. G. Oas, *Proc. Natl. Acad. Sci. U. S. A.*, 2009, **106**, 13737–13741; (*c*) A. D. Vogt and E. di Cera, *Biochemistry*, 2012, **51**, 5894–5902.

46 (*a*) L. C. James and D. S. Tawfik, *Trends Biochem. Sci.*, 2003, **28**, 361–368; (*b*) D. D. Boehr, R. Nussinov and P. E. Wright, *Nat. Chem. Biol.*, 2009, **5**, 789–796; (*c*) P. Csermely, R. Palotai and R. Nussinov, *Trends Biochem. Sci.*, 2010, **35**, 539–546.

47 Y. Sakata, M. Okada and S. Akine, *Chem. – Eur. J.*, 2021, **27**, 2284–2288.

48 B. Zhang, H. Lee, J. J. Holstein and G. H. Clever, *Angew. Chem., Int. Ed.*, 2024, **63**, e202404682.

49 D. A. McMorran and P. J. Steel, *Angew. Chem., Int. Ed.*, 1998, **37**, 3295–3297.

50 (*a*) W. M. Bloch and G. H. Clever, *Chem. Commun.*, 2017, **53**, 8506–8516; (*b*) S. Pullen, J. Tessarolo and G. H. Clever, *Chem. Sci.*, 2021, **12**, 7269–7293.

51 (*a*) W. M. Bloch, Y. Abe, J. J. Holstein, C. M. Wandtke, B. Dittrich and G. H. Clever, *J. Am. Chem. Soc.*, 2016, **138**, 13750–13755; (*b*) W. M. Bloch, J. J. Holstein, W. Hiller and G. H. Clever, *Angew. Chem., Int. Ed.*, 2017, **56**, 8285–8289.

52 (*a*) S. Akine, M. Miyashita, S. Piao and T. Nabeshima, *Inorg. Chem. Front.*, 2014, **1**, 53–57; (*b*) S. Akine, M. Miyashita and T. Nabeshima, *Inorg. Chem.*, 2021, **60**, 12961–12971.

53 S. A. Ikbal, P. Zhao, M. Ehara and S. Akine, *Sci. Adv.*, 2023, **9**, eadj5536.

54 For related oligo(salen)/oligo(saloph) cages, see: (*a*) S. Akine, S. Piao, M. Miyashita and T. Nabeshima, *Tetrahedron Lett.*, 2013, **54**, 6541–6544; (*b*) S. M. Elbert, F. Rominger and M. Mastalerz, *Chem. – Eur. J.*, 2014, **20**, 16707–16720; (*c*) J. Jiao, C. Tan, Z. Li, Y. Liu, X. Han and Y. Cui, *J. Am. Chem. Soc.*, 2018, **140**, 2251–2259; (*d*) S. M. Elbert, W.-S. Zhang, Y. Vaynzof, N. Oberhof, M. Bernhardt, M. Pernpointner, F. Rominger, R. R. Schröder and M. Mastalerz, *Chem. Mater.*, 2019, **31**, 6210–6223; (*e*) Y. Sakata, R. Tsuyuki, S. Sugimoto and S. Akine, *Chem. Commun.*, 2021, **57**, 13510–13513; (*f*) F. Uhrmacher, S. M. Elbert, F. Rominger and M. Mastalerz, *Eur. J. Inorg. Chem.*, 2022, e202100864; (*g*) S. Firdausiah, R. Ide, M. Ehara, P. Zhao, Y. Sakata and S. Akine, *Chem. – Eur. J.*, 2025, **31**, e202501277.

55 Y. Sakata, S. Chiba, M. Miyashita, T. Nabeshima and S. Akine, *Chem. – Eur. J.*, 2019, **25**, 2962–2966.

56 (*a*) H. Miyake and H. Tsukube, *Chem. Soc. Rev.*, 2012, **41**, 6977–6991; (*b*) S. Akine, *Inorganics*, 2018, **6**, 80; (*c*) S. Akine and H. Miyake, *Coord. Chem. Rev.*, 2022, **468**, 214582; (*d*) S. Akine, *Pure Appl. Chem.*, 2023, **95**, 331–341.

57 Recent examples of chirality control of metal complexes, see: (*a*) S. Akine, T. Taniguchi and T. Nabeshima, *Tetrahedron Lett.*, 2006, **47**, 8419–8422; (*b*) S. Akine, T. Matsumoto and T. Nabeshima, *Chem. Commun.*, 2008, 4604–4606; (*c*) S. Akine, S. Hotate, T. Matsumoto and T. Nabeshima, *Chem. Commun.*, 2011, **47**, 2925–2927; (*d*) S. Akine, S. Hotate and T. Nabeshima, *J. Am. Chem. Soc.*,

2011, **133**, 13868–13871; (*e*) S. Akine, S. Sairenji, T. Taniguchi and T. Nabeshima, *J. Am. Chem. Soc.*, 2013, **135**, 12948–12951; (*f*) S. Sairenji, S. Akine and T. Nabeshima, *Tetrahedron Lett.*, 2014, **55**, 1987–1990; (*g*) S. Sairenji, S. Akine and T. Nabeshima, *Chem. Lett.*, 2014, **43**, 1107–1109; (*h*) S. Akine, T. Matsumoto and T. Nabeshima, *Angew. Chem., Int. Ed.*, 2016, **55**, 960–964; (*i*) S. Sairenji, S. Akine and T. Nabeshima, *Dalton Trans.*, 2016, **45**, 14902–14906; (*j*) S. Sairenji, S. Akine and T. Nabeshima, *Sci. Rep.*, 2018, **8**, 137; (*k*) S. Akine, K. Nomura, M. Takahashi, Y. Sakata, T. Mori, W. Nakanishi and K. Ariga, *Dalton Trans.*, 2023, **52**, 260–268; (*l*) S. Muratsugu, K. Sawaguchi, T. Shiraogawa, S. Chiba, Y. Sakata, S. Shirai, H. Baba, M. Ehara, S. Akine and M. Tada, *Chem. Commun.*, 2024, **60**, 2094–2097.

58 Y. Sakata, S. Chiba and S. Akine, *Proc. Natl. Acad. Sci. U. S. A.*, 2022, **119**, e2113237119.

59 S. Akine and Y. Sakata, *Chem. Lett.*, 2020, **49**, 428–441.

60 (*a*) E. L. Piatnitski and K. D. Deshayes, *Angew. Chem., Int. Ed.*, 1998, **37**, 970–972; (*b*) S. Zarra, M. M. J. Smulders, Q. Lefebvre, J. K. Clegg and J. R. Nitschke, *Angew. Chem., Int. Ed.*, 2012, **51**, 6882–6885; (*c*) H. Wang, F. Liu, R. C. Helgeson and K. N. Houk, *Angew. Chem., Int. Ed.*, 2013, **52**, 655–659.

61 S. Akine, M. Miyashita and T. Nabeshima, *J. Am. Chem. Soc.*, 2017, **139**, 4631–4634.

62 S. Akine, M. Miyashita and T. Nabeshima, *Chem. – Eur. J.*, 2019, **25**, 1432–1435.

63 S. P. Black, J. K. M. Sanders and A. R. Stefankiewicz, *Chem. Soc. Rev.*, 2014, **43**, 1861–1872.